[11] K. Kanatani, "Analysis of 3-D rotation fitting," *IEEE Trans. Pattern Anal. Mach. Intell.*, vol. 16, no. 5, pp. 543–549, 1994.
[12] S. Krishnan, P. Y. Lee, J. B. Moore, and S. Venkatasubramanian, "Global registration of multiple 3D point sets via optimization-on-a-manifold," in *Proc. Eurographics Symp. Geometry Processing*, 2005, pp. 1–11.
[13] Y. H. Liu, "Improving ICP with easy implementation for free-form surface matching," *Pattern Recogn.*, vol. 37, pp. 211–226, 2004.
[14] B. D. Lucas and T. Kanade, "An iterative image registration technique with an application to stereo vision," in *Proc. 7th Int. Joint Conf. Arti. Intell.*, 1981, pp. 121–130.
[15] X. Pennec and J. P. Thirion, "A framework for uncertainly and validation of 3D registration methods based on points and frames," *Int. J. Comput. Vision*, vol. 25, no. 3, pp. 203–229, 1997.
[16] B. M. Planitz, A. J. Maeder, and J. A. Williams, "The correspondence framework for 3D surface matching algorithm," *Computer Vision and Image Understanding*, vol. 97, pp. 347–383, 2005.
[17] H. Pottmann and M. Hofer, "Geometry of the squared distance function to curves and surface," in *Visualization and Mathematics III*, H. C. Hege and K. Polthier, Eds. New York: Springer, 2003, pp. 221–242.
[18] H. Pottmann, Q. X. Huang, Y. L. Yang, and S. M. Hu, "Geometry and convergence analysis of algorithms for registration of 3D shapes," *Int. J. Comput. Vision*, vol. 67, no. 3, pp. 277–296, 2006.
[19] S. Rusinkiewicz and M. Levoy, "Efficient variants of ICP algorithm," in *Proc. 3rd Int. Conf. 3D Digital Imaging and Modeling*, 2001, pp. 145–152.
[20] G. C. Sharp, S. W. Lee, and D. K. Wehe, "ICP registration using invariant features," *IEEE Trans. Pattern Anal. Mach. Intell.*, vol. 24, no. 1, pp. 90–102, 2002.
[21] S. Umeyama, "Least-squares estimation of transformation parameters between two point patterns," *IEEE Trans. Pattern Anal. Mach. Intell.*, vol. 13, no. 4, pp. 376–380, 1991.
[22] P. Yan and K. W. Bowyer, "A fast algorithm for ICP-based 3D shape biometrics," in *Proc. 4th IEEE Workshop on Autom. Identif. Adv. Technol.*, 2005, pp. 213–218.
[23] Z. Zhang, "Iterative point matching of free-from curves and surfaces," *Int. J. Comput. Vision*, vol. 13, no. 2, pp. 119–152, 1994.
[24] T. Zinßer, J. Schmidt, and H. Niemann, "A refined ICP algorithm for robust 3-D correspondence estimation," in *Proc. 2003 Int. Conf. Image Process.*, 2003, pp. 695–698.
[25] B. Zitová and J. Flusser, "Image registration methods: A survey," *Image and Vision Comput.*, vol. 21, pp. 977–1000, 2003.

# Visual-Based Impedance Control of Out-of-Plane Cell Injection Systems

Haibo Huang, Dong Sun, James K. Mills, Wen J. Li, and Shuk Han Cheng

***Abstract*—In this paper, a vision-based impedance control algorithm is proposed to regulate the cell injection force, based on dynamic modeling conducted on a laboratory test-bed cell injection system. The injection force is initially calibrated to derive the relationship between the force and the cell deformation utilizing a cell membrane point-load model. To increase the success rate of injection, the injector is positioned out of the focal plane of the camera, used to obtain visual feedback for the injection process. In this out-of-plane injection process, the total cell membrane deformation is estimated, based on the $X - Y$ coordinate frame deformation of the cell, as measured with a microscope, and the known angle between the injector and the $X - Y$ plane. Further, a relationship between the injection force and the injector displacement of the cell membrane, as observed with the camera, is derived. Based on this visual force estimation scheme, an impedance control algorithm is developed. Experimental results of the proposed injection method are given which validate the approach.**

***Note to Practitioners*—In biological cell injection, the control of injection forces is important since excessive manipulation force may destroy the membrane or tissue of the biological cell, and lead to failure of the biomanipulation task. Although the injection force is a very important factor that affects the survivability of the injected cells, research on minimally invasive cell injection, based on understanding of the mechanical properties of the cellular membrane, are rare. To resolve this problem, a methodology is presented here to regulate cell injection forces using geometry of cell deformations and micro vision feedback. With the visually measured injection force applied to an injected cell, an impedance control strategy is then developed to regulate the cell injection force through the desired impedance. One advantage of using the impedance control in micromanipulation is that tiny forces exerted on the cell membrane can be reflected in the control system by adjusting the controller impedance coefficients.**

***Index Terms*—Biomanipulation, cell injection, impedance control, microrobotic system.**

## I. Introduction

Since its invention during the first half of the last century, biological cell injection has been widely applied in gene injection [1], *in-vitro* fertilization (IVF) [2], intracytoplasmic sperm injection (ISCI) [3], and drug development [4]. Until very recently, however, existing research

Manuscript received August 13, 2007; revised November 22, 2007. First published May 12, 2009; current version published July 01, 2009. This paper was recommended for publication by Associate Editor M. Zhang and Editor D. Meldrum upon evaluation of the reviewers' comments. This work was supported by a grant from the Research Grants Council of the Hong Kong Special Administrative Region, China (Reference No. CityU 119705) and a grant from the City University of Hong Kong (Project No. 7002461).

H. B. Huang was with the Department of Manufacturing Engineering and Engineering Management, City University of Hong Kong, Kowloon, Hong Kong. He is now with the Department of Mechanical and Industrial Engineering, University of Toronto, Toronto, ON M5S 3G8, Canada (e-mail: hbhuang@mie.utoronto.ca).

D. Sun is with the Department of Manufacturing Engineering and Engineering Management, City University of Hong Kong, Kowloon, Hong Kong (e-mail: medsun@cityu.edu.hk).

J. K. Mills is with the Department of Mechanical and Industrial Engineering, University of Toronto, Toronto, ON M5S 3G8, Canada (e-mail: mills@mie.utoronto.ca).

W. J. Li is with the Centre for Micro and Nano Systems, Chinese University of Hong Kong, Shatin, NT, Hong Kong (e-mail: wen@acae.cuhk.edu.hk).

S. H. Cheng is with the Department of Biology and Chemistry, City University of Hong Kong, Kowloon, Hong Kong (e-mail: bhcheng@cityu.edu.hk).

Digital Object Identifier 10.1109/TASE.2008.2010013

towards solutions to the cell injection problem [2], [5], [6] have been unable to fulfill the expectations of the industry. Most cell injection operations are currently performed manually. Furthermore, studies indicate that skilled operators require up to one year of training and can achieve a success rate of only 15% for these transgenic tasks (gene injection into cells) [1]. In addition, most manual cell injection processes are neither accurate nor repeatable. Hence, there exists an increasing demand for an accurate and reliable cell injection system and methodology so that large batch biomanipulation production can be realized.

During the process of cell injection, the injection force is an important factor that affects the survivability of the injected cells. Accurate measurement and control of the cell injection force helps improve the overall performance of the cell injection process. Recently, research work has been performed to determine the forces involved in the cell injection. Research on bonding a microinjection pipette on the tip of a polyvinylidene fluoride (PVDF) film force sensor to detect the injection forces in fish egg biomanipulation was performed in [7]–[9]. A microelectromechanical system (MEMS)-based two-axis cellular force sensor was developed in [10] to investigate the mechanical properties of mouse oocyte zona pellucida. A micrograting-based injection force sensor with a surface micromachined silicon-nitride injector was used in [11]. A monolithically fabricated micro-gripper with integrated force sensor was reported for manipulating micro-objects and biological cells aligned in an ultrasonic field [12].

Visual-based force control [13]–[17] has been developed to estimate forces applied to a linearly elastic object using the contour data, based on visual data. This approach utilizes microscope optics and digital cameras that are standard components of a micromanipulation or biomanipulation workstation. Hence, this hardware, required in the proposed and other systems, does not add to the complexity of the micromanipulation system.

In this paper, a cell injection system with force-feedback regulation is proposed for cell injection tasks. Preliminary results of the work presented in this paper appeared in [18]. The process considered here is for injection of genetic material into a cell with the injector pipette positioned out (tilt at an angle) of the focal plane of the camera used to image the process, i.e., this process is termed out-of-plane injection. This approach provides several advantages over injection in which the injector is in the same plane as the microscope. First, the injection pipette is separated vertically such that transfer to the next cell for injection readily avoids a collision between the cell and pipette. Second, the cells are held by a specially designed cell holder [19], eliminating the need for a holding tube. Third, by contacting the cells out of the plane, the cells are not simply brushed aside by the injector pipette, but can achieve a successful injection. This injection process is similar to the process used in automatic adherent cell injection [1]. A study on mechanical modeling of injected cells was reported in [20].

Fig. 1 illustrates the laboratory test-bed cell injection system in which the injector tilted at an angle to the plane of a $X-Y$ positioning table is shown. In the following, we demonstrate that the injector force can be determined by measuring the deformation of the cell membrane in the $X-Y$ plane, and by knowing various other parameters, including the angle the injector makes with respect to the $X-Y$ plane. During an out-of-plane injection task, the total cell deformation is generally difficult to measure directly, since the injector is not in the camera focal plane, i.e., here the $X-Y$ plane. With calibration of the cell membrane mechanical properties performed with the injector positioned in the same plane as the microscope focal plane, we are able to derive the relationship between the force imparted by the injection pipette and the resulting cell membrane deformation. The cell deformation is estimated based on the distance the injector deforms the cell membrane, projected into the $X-Y$ plane, as measured with the microscope, and the known angle the injector makes relative to the $X-Y$ plane. With the estimated injection force, an impedance control strategy is then developed, in a similar manner to [21]. One advantage of the impedance control in micromanipulation is that tiny forces exerted on the cell membrane can be reflected in the control system by adjusting the controller impedance coefficients. Injector motion planning is also designed in this study. Finally, experiments are performed to demonstrate the effectiveness of the proposed approach.

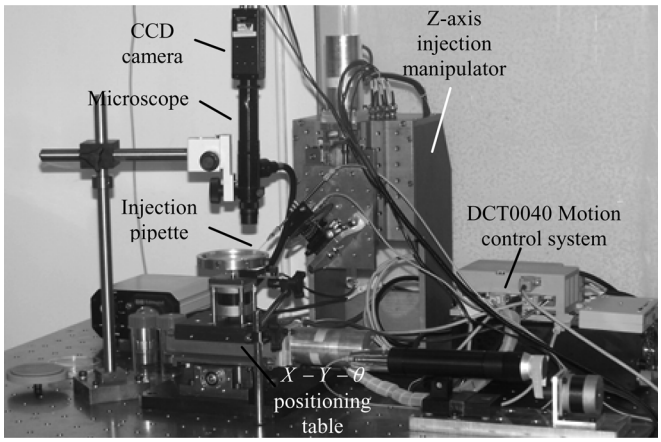


Fig. 1. Laboratory test-bed cell injection system.

The major contributions of this work are twofold. First, we propose a novel methodology to use planar visual feedback to estimate cell deformation and therefore the injection force. Second, we propose to use an impedance control algorithm to regulate the injection force during the cell injection.

## II. System Setup and Dynamic Modeling

The cell injection system, as shown in Fig. 1, is designed to simulate automatic cell injection of large batches of cells in biological engineering, in which the cells are transported by a rotary table, one by one, into the injection field, for injection with a pipette [18].

The system consists of an $X-Y-\theta$ positioning table and the injection manipulator mounted so that it may travel in the $Z$ axis direction. Embryo cells which are to be injected are placed in a cell holder, which is fixed to a rotary table, mounted on the $X-Y-\theta$ positioning table. Coordinated motion of the axes of the $X-Y-\theta$ table and the $Z$ axis injector is required to perform the cell injection task. The $X-Y$ stage has a workspace of 60 mm $\times$ 60 mm, with a positional resolution of 0.3175 $\mu$m in each axial direction. The $Z$ axis stage has a maximum displacement of 50 mm, and a positional resolution of 0.3175 $\mu$m. The injector pipette is oriented at a fixed angle $\varphi$ with respect to the $X-Y$ plane. The $X$, $Y$, and $Z$ axes are driven by DC brushless motors with embedded encoders. The vision system is comprised of four components: an optical microscope, CCD camera, PCI image capture and processing card, and image processing computer. The Mitutoyo Optical Microscope has a working distance of 2 cm to provide sufficient space for micromanipulation. The PULNIX TM-6701AN Progressive Scan camera and the NI 1409 image capture card have a high image capture frequency of 60 Hz to observe the cell injection process. The control module consists of a host computer (PD 2.8 GHz) and a motion control/drive system provided by DynaCity Technology HK, Ltd.

The modeling of the above microinjection system is presented in detail in [18]. However, here, we provide sufficient details to enhance the readability of this paper. The coordinate frame $O-XYZ$ is defined with its origin $O$ located at the center of the working plate, located below the microscope. A microscope is mounted above the point at which embryo insertions are to be made, with its optical axis coincident

with the $Z$ axis coordinate direction. The camera coordinate frame, with $O_c$ located at the center of the camera, and $Z_c$ coincident with the optical axis of the microscope, is defined as $O_c - X_cY_cZ_c$. $O_i - uv$ is defined as the image plane coordinate frame, with coordinates $u$, $v$ and $\theta_i$. The origin of this frame, denoted by $O_i$, is coincident with the optical axis, and the axes $u$ and $v$ define the camera image plane, which is oriented perpendicular to the optical axis.

The relationship between coordinates $[u,v,Z,\theta_i]^T$ and $[X, Y, Z, \theta]^T$ is given as

$$\begin{aligned}\begin{bmatrix} u \\ v \\ Z \\ \theta_i \end{bmatrix} &= \begin{bmatrix} f_X\cos\alpha & f_X\sin\alpha & 0 & 0 \\ -f_Y\sin\alpha & f_Y\cos\alpha & 0 & 0 \\ 0 & 0 & 1 & 0 \\ 0 & 0 & 0 & 1 \end{bmatrix} \begin{bmatrix} X \\ Y \\ Z \\ \theta \end{bmatrix} \\ &\quad + \begin{bmatrix} f_X d_X \\ f_Y d_Y \\ 0 \\ 0 \end{bmatrix} \\ &= T \begin{bmatrix} X \\ Y \\ Z \\ \theta \end{bmatrix} + \begin{bmatrix} f_X d_X \\ f_Y d_Y \\ 0 \\ 0 \end{bmatrix} \end{aligned} \tag{1}$$

where $T \in \Re^{4\times4}$ is the transformation matrix between the image frame and the stage frame. Since the both frames are fixed, $T$ is time-invariant and hence $f_X$, $f_Y$, $d_X$, $d_Y$ are constant parameters.

The dynamic equations of motion of the four DOF motion stage, developed with Lagrange's equations, is given as in

$$M\ddot{q} + N\dot{q} + G = \tau - \begin{bmatrix} J^T f_e \\ 0 \end{bmatrix} \tag{2}$$

where $q = [X,Y,Z,\theta]^T$ are the task space coordinates, $M = \begin{bmatrix} m_X + m_Y + m_p & 0 & 0 & 0 \\ 0 & m_Y + m_p & 0 & 0 \\ 0 & 0 & m_Z & 0 \\ 0 & 0 & 0 & I_P \end{bmatrix} T^{-1}$ is the inertia matrix of the system, $m_X$, $m_Y$ and $m_Z$ are the masses of the $X$, $Y$ and $Z$ positioning tables, respectively, $m_p$ is the mass of the working table, $I_p$ is the rotational inertia of the rotary axis and the working table, $N \in \Re^{4\times4}$ denotes a diagonal matrix of the positioning table damping and viscous friction coefficients, and $G = [0,0,-m_Z g,0]^T$ is the gravitational force vector, $\tau = [\tau_X,\tau_Y,\tau_Z,\tau_r]^T$ is the torque input to the driving motors, $J$ is the Jacobian matrix relating task and joint coordinates and $f_e = [f_{eX},f_{eY},f_{eZ}]^T$ represents the cell injection forces applied to the actuators during the injection process. Note that the rotation angle $\theta$ does not change during this process, hence, only forces in the three Cartesian coordinate directions need to be considered.

## III. Injection Controller Design

### A. Injector Motion Profile

An injection motion trajectory must be designed for the cell injection tasks. Fig. 2 illustrates the proposed out of plane cell injection process. Note that prior to initiation of the process, the injector may be located at a $Z$ coordinate position that it is not observed by the microscope. Consequently, the injector must move in the $Z$ axis direction, to permit the injector to be imaged by the microscope. Let $q_a$ be defined as the vertical displacement of the injector tip prior to initiation of the process. The injector tip is first translated to a predetermined injection $Z$-coordinate that places the injector tip within the focal range of the microscope. The injector tip then comes to rest at vertical displacement $q_b$, using a visual guided servoing approach. The movement of the injector and deformation of the cell membrane in the $X - Y$ plane can

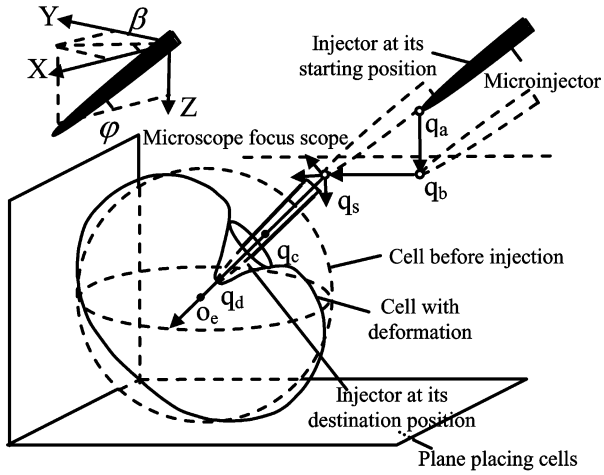


Fig. 2. Out-of-plane cell injection process.

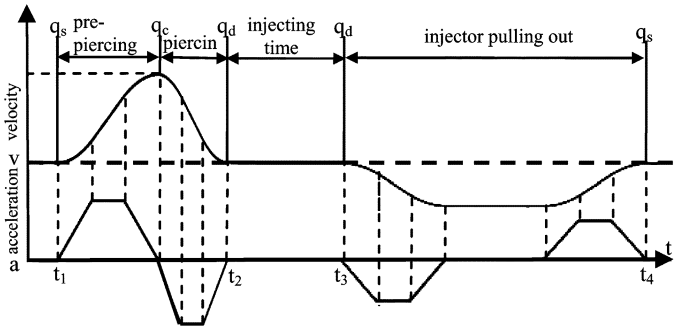


t1–time at the starting position qs; t2–time before injection at qd;
t3–time after injection at qd; t4–time after pulling out injector at qs.

Fig. 3. Velocity and acceleration profiles of injector during the injection process.

now be observed by the microscope. Utilizing a visual servo method proposed in this work, the injector tip is translated towards the starting injection position $q_s$. The injector tip is then accelerated towards the embryo, in a prepiercing step. The injector motion must be carried out so that its motion of the pipette is directed along the longitudinal axis of the pipette, and also towards the center of the cell, denoted by $o_e$. To achieve this motion, the $X$, $Y$, and $Z$ axes must move in a coordinated manner. With the proposed motion profile, the injector tip velocity is designed to be at its highest value at the moment the tip reaches the cell membrane, to successfully piece the cell membrane. This occurs at when the injector reaches position $q_c$. The injector is then decelerated to allow the smooth approach to the desired injection position $q_d$, at which point material is injected into the cell. Following this step, the injector is accelerated, in the opposite direction, removing the injector form the interior of the cell and exiting the cell membrane. The velocity and acceleration profiles of the injector, starting from the prepiercing step at $q_s$ and terminating at the same coordinate $q_s$, are shown in Fig. 3.

### B. Cell Injection Force Estimation

It is proposed to estimate the force applied by the out of plane injector pipette by utilizing visual feedback of the cell wall deformation in the plane, coupled with the dynamic parameters of the dynamic model of the cell wall. This estimation procedure is described below in a four stage procedure.

*1) Stage (i):* We utilize a planar injection method for calibration, carried out in the $X - Y$ plane ($\varphi = 0$), different than the out of plane

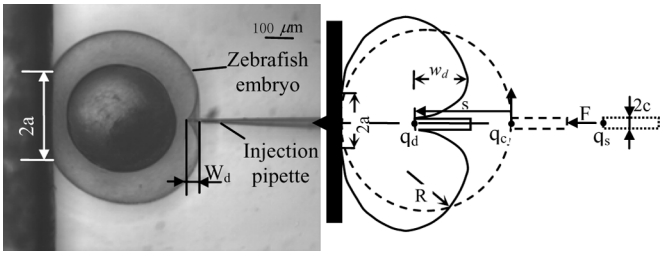


Fig. 4. Horizontal cell injection force calibration with cell membrane point-load model.

injection process described previously. With the injector pipette positioned in the microscope focal plane, the injection force is calibrated utilizing the cell membrane point model given in [10]. The relationship between the cell injection force $F$ and the cell membrane deformation $w_d$ can then be derived.

Note that during the out of plane cell injection process, the geometric change of the cell membrane in the $Z$ axis coordinate direction cannot be detected by the microscope. To solve this problem, we propose to utilize the deformation of the cell, as observed in the $X-Y$ plane, to estimate the total cell membrane deformation. This approach is valid for the case in which the angle between the $Z$ axis injector pipette and the $X-Y$ plane is known, and also, under the assumption that batches of cells have similar membrane dynamic characteristics at similar development stages [22].

For this calibration, experiments are conducted with the injector pipette placed in the $X-Y$ plane, as shown in Fig. 4. The cell injection force is then estimated using the membrane point-load model [10]. The pipette with radius $c$ exerts a force $F$ on the membrane, creating a dimple with a radius $a$ and depth $w_d$ and semicircular curved surface with a radius $R$. The cell injection force is then calculated using the following equation taken from [10]:

$$F = \frac{2\pi E h \mathrm{w}_d^3}{a^2(1-\gamma)}\left[\frac{3-4\zeta^2+\zeta^4+2\ln\zeta^2}{(1-\zeta^2)(1-\zeta^2+\ln\zeta^2)^3}\right] \tag{3}$$

where $E$ is the membrane elastic modulus, $\gamma$ is the Poisson ratio, $h$ is the thickness of the membrane, and $\zeta = c/a$, $c$ is the radius of the injector. In the above equation, membrane material parameters $E$ and $\gamma$ and dimensions $h$ and $c$ are constants, while $a$ and $w_d$ are variables obtained from microscope images.

*2) Stage (ii):* The relationship between the cell injection force $F$, the injector distance $s$, and the cell membrane deformation $w_d$ is determined from the $X-Y$ plane calibration cell injection experiments. In other words, the injection force $F$ may be estimated from the injector penetration distance $s$. In practice, the parameter $w_d$ is more difficult to obtain than the distance the injector has moved inside the undeformed cell membrane boundary, i.e., from $q_c$ to $q_d$, denoted as $s$ in Fig. 4. Through a series of calibration experiments, the relationship of the cell injection force $F$ to the injector penetration distance $s$ inside the cell can be obtained. Then, the injection force $F$ may be determined given the distance the injector has moved inside the undeformed cell wall boundary, $s$, instead of. $w_d$.

*3) Stage (iii):* In out-of-plane injection tasks, the injector distance in $X-Y$ plane observed by the microscope, is used to estimate the injector distance $s$ in three dimensions, under the condition that the tilt angle, $\varphi$, of the injector is known.

The distance of the injector inside the cell is expressed as

$$s = \sqrt{(X-X_{qc})^2+(Y-Y_{qc})^2+(Z-Z_{qc})^2} \tag{4}$$

where $X_{qc}$, $Y_{qc}$ and $Z_{qc}$ are coordinates at the contact point $q_c$, as shown in Fig. 2; $\begin{bmatrix} X \\ Y \end{bmatrix} = T_{xy}^{-1}\begin{bmatrix} u-u_{qc} \\ v-v_{qc} \end{bmatrix}$, $[u,v]^T$ is the image coordinate of the injector pipette head, and $[u_{qc}, v_{qc}]^T$ is the image coordinate of the point $q_c$. The deformation $Z-Z_{qc}$ cannot be detected by the microscope directly. It can be derived based on the deformations in the $X$ and $Y$ coordinate directions and the tilt angle $\varphi$. As a result, (4) can be rewritten as shown in (5) at the bottom of the page.

*4) Stage (iv):* Finally, the cell injection force $F$ in three dimensions is estimated based on relationship in stage (ii).

### C. Impedance Control in Cell Injection

Impedance control achieves desired dynamic response of a system by controlling its impedance to a desired value and is robust to model uncertainties and external disturbance. In order to regulate the cell injection force during the injection process, an impedance control methodology incorporated by the visual-based injection force estimation is developed here.

The contact space impedance control is given as

$$m\ddot{e} + b\dot{e} + ke = f_e \tag{6}$$

where $m$, $b$, and $k$ are the desired impedance parameters, $e = [X^d, Y^d, Z^d]^T - [X, Y, Z]^T$, representing the position errors of the $X-Y$ stage and the $Z-$ axis injector. The external force $f_e$ applied to the actuator is expressed as

$$f_e = -\begin{bmatrix} F_X \\ F_Y \\ F_Z \end{bmatrix} = -F\cdot\begin{bmatrix} \cos(90^\circ-\varphi)\cdot\cos\beta \\ \cos(90^\circ-\varphi)\cdot\sin\beta \\ \sin(90^\circ-\varphi) \end{bmatrix} \tag{7}$$

where $\beta$ is the angle between the injector and $X$ axis. Both $\beta$ and the tilt angle $\varphi$ are fixed during the injection process.

Solve $[\ddot{X},\ddot{Y},\ddot{Z}]^T$ from (6) as follows:

$$\begin{bmatrix} \ddot{X} \\ \ddot{Y} \\ \ddot{Z} \end{bmatrix} = m^{-1}\left(m\begin{bmatrix} \ddot{X}^d \\ \ddot{Y}^d \\ \ddot{Z}^d \end{bmatrix} + b\dot{e} + ke - f_e\right). \tag{8}$$

Substituting (8) into (2) yields an image-based three-dimensional torque controller as follows:

$$\tau_{XYZ} = M_{XYZ}\left(\begin{bmatrix} \ddot{X}^d \\ \ddot{Y}^d \\ \ddot{Z}^d \end{bmatrix} + m^{-1}(b\dot{e}+ke-f_e)\right) + N_{XYZ}\begin{bmatrix} \dot{X} \\ \dot{Y} \\ \dot{Z} \end{bmatrix} + G_{XYZ} + J^T f_e \tag{9}$$

where the matrices $M_{XYZ}$, $N_{xyz}$ and $G_{xyz}$ are submatrices of $MT$, $NT$ and $G$ corresponding to $X$, $Y$ and $Z$ axes, respectively, and $f_e$

$$s = \sqrt{(X-X_{qc})^2+(Y-Y_{qc})^2+\left(\frac{\sqrt{(X-X_{qc})^2+(Y-Y_{qc})^2}}{\sin\varphi}\right)^2} \tag{5}$$

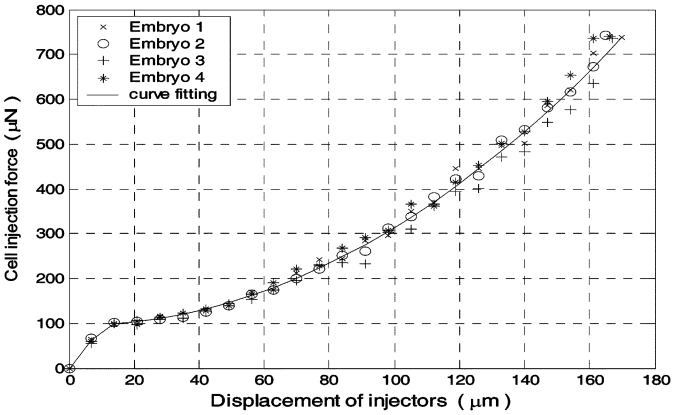


Fig. 5. Cell injection force calibration.

is the actual injection force that can be determined according to the injector moving distance inside the cell. The cell injection force can be regulated through the desired impedance.

## IV. Experimental Procedure and Results

In this section, we discuss experiments which were performed using the experimental equipment illustrated in Fig. 1. The dynamic model parameters of the system have been estimated based on geometric data and calibration experiments reported in [18]. The calibrated values of the inertia, viscous friction matrices and gravity vector are presented in [18], hence are not given here. The angle between the injector and the $X$ axis is $\beta = 45^\circ$. The tilt angle is $\varphi = 35.26^\circ$. From (7), we then have $f_e = -\left[\sqrt{3}/3, \sqrt{3}/3, \sqrt{3}/3\right]^T F$.

Zebrafish embryos are used for demonstration of the injection system process, as Zebrafish is a commonly used animal model due to its genetic similarity to higher vertebrates. Further, the Zebrafish eggs are easily obtained, exhibit short generation time, require external fertilization and have translucent embryos [7]. The diameter of the Zebrafish egg is approximately 1.15–1.25 mm (including chorion). The Poisson ratio $\gamma = 0.5$ and the thickness of the membrane $h = 3\ \mu\mathrm{m}$, with the radius of the injector $c = 6.4\ \mu\mathrm{m}$. As the membrane of the Zebrafish embryos undergoes a "chorion softening" process during early development, the membrane elastic modulus $E$ varies with time, following fertilization and also exhibits variation during subsequent development stages. Quantitative measurement of the elastic modulus change was carried out in [22]. In our experiments, the Zebrafish embryos were all injected at blastula stage and at this stage the membrane elastic modulus is $E = 1.51\ \mathrm{MPa}$.

### A. Force Calibration

Calibration experiments were carried out to estimate the relation between the cell injection force $F$ and the injector penetration distance inside the cell, denoted by $s$ as given in (3) taken from [10]. Significantly, these experiments are also used to verify that the mechanical properties of the cell membrane are similar from cell to cell of similar stages of development. These calibrations were conducted on a number of cells, with the injector pipette located in the $X - Y$ plane with the pipette moving in an axial direction towards the center of the cell. The

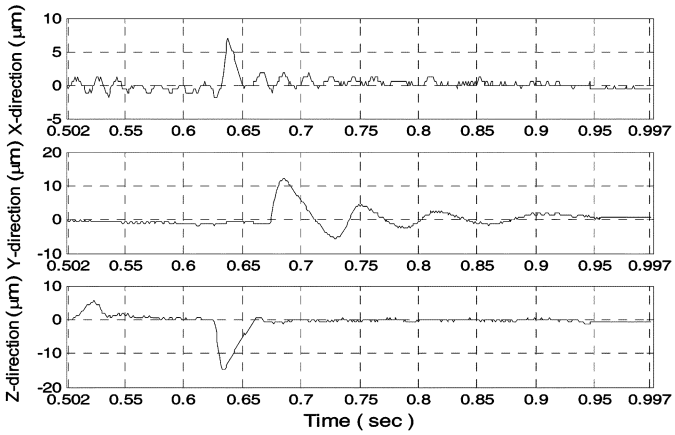


(a) Position error of injector in three axes

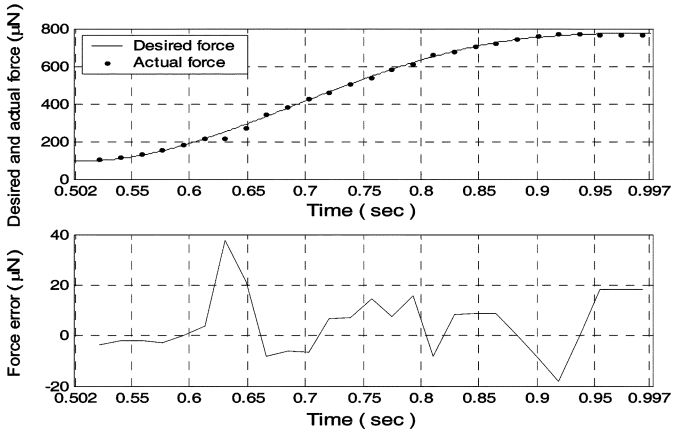


(b) Injection force and injection force error

Fig. 6. Experimental results with the PID control. (a) Position error of injector in three axes. (b) Injection force and injection force error.

distances $s$ and $w_d$ were measured directly from images taken. $F$ was then calculated using (3). A micro-force sensor was utilized to calibrate the force-displacement relationship. Fig. 5 illustrates typical experimental results obtained using four embryos, where the horizontal axis denotes the injector distance $s$, and the vertical axis denotes the calculated cell injection force $F$. Based on this relationship, the cell injection force $F$ can be directly estimated from the injector distance $s$ instead of the cell membrane deformation $w_d$, i.e., see (10) at the bottom of the page.

### B. Motion Planning

It was found out in our planar injection experiments, most of the membrane of Zebrafish embryo (blastula stage) were punctured when the insertion distance $s$ exceeds 170 $\mu$m. Therefore, the motion trajectory was planned based on an injection distance not less than 170 $\mu$m. In our experiments, the desired injection distance was 175 $\mu$m, and the desired pre-piercing movement distance was 175 $\mu$m. Both the desired velocity and position profiles of the injector were designed according to Fig. 3. For details, please see [18].

$$F = \begin{cases} 8.5714s, & 7\ \mu\mathrm{m} > s > 0 \\ 0.02274 \cdot s^2 - 0.09252 \cdot s + 95.31, & 170\ \mu\mathrm{m} > s > 7\ \mu\mathrm{m} \\ 0, & s > 170\ \mu\mathrm{m} \end{cases} \tag{10}$$

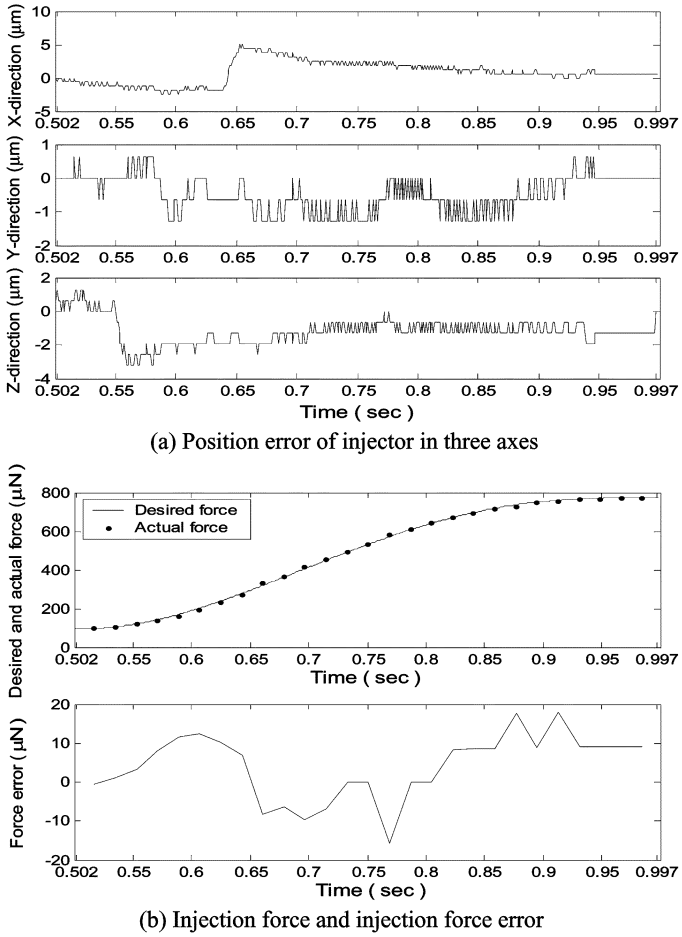


(a) Position error of injector in three axes

(b) Injection force and injection force error

Fig. 7. Experimental results with the computed torque control. (a) Position error of injector in three axes. (b) Injection force and injection force error.

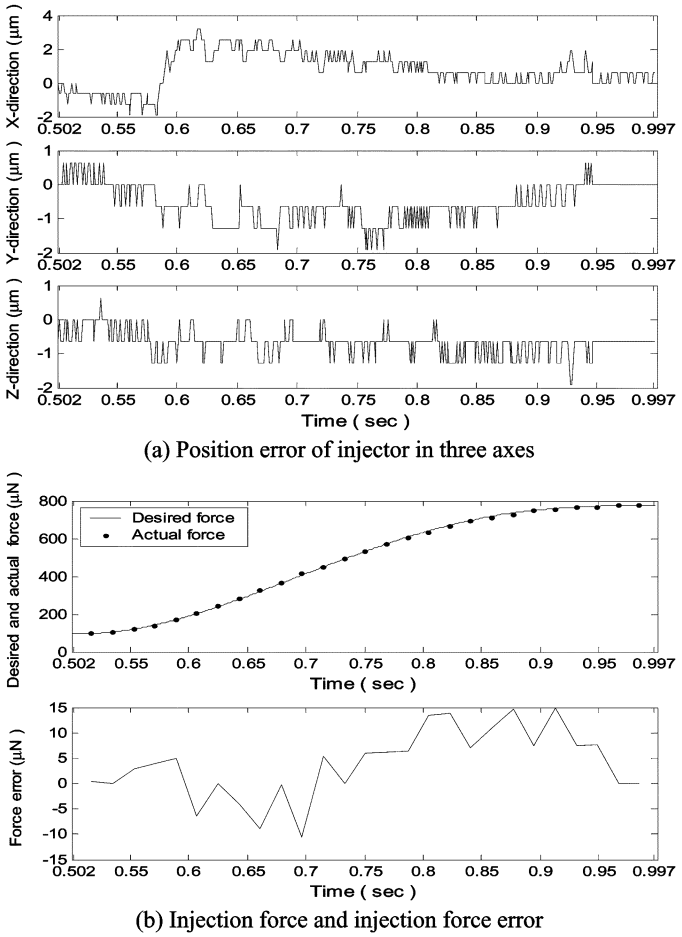


(a) Position error of injector in three axes

(b) Injection force and injection force error

Fig. 8. Experimental results with the vision-based impedance force control. (a) Position error of injector in three axes. (b) Injection force and injection force error.

### C. Experimental Results

Three different control methods were used in the experiments, for comparison purposes. The embryo cells used were collected in accordance with standard embryo preparation procedures. After being placed at room temperature for two hours after fertilization (blastula stage), with the mechanical properties of membrane uniform and stable, all Zebrafish embryos, of similar size, were injected. Close control over the process of preparation of the embryos for injection, ensures the validity of the assumption that all embryo cells used in our experiments exhibited the similar dynamic characteristics. The experimental results during the piercing period of the injection process ($0.5\ \text{sec} < t < 1\ \text{sec}$) are shown below.

Fig. 6 illustrates experimental results with a standard PID control. The PID control gains were chosen as $k_p = \text{diag}\{0.6012,0.6012,0.6914\} \times 10^6\ \text{N}$, $k_d = \text{diag}\{0.1503,0.1203,0.1503\} \times 10^3\ \text{N}\cdot\text{s}$, and $k_i = \text{diag}0.3006,0.3608,0.3903\} \times 10^8\ \text{N/s}$. Fig. 6(a) shows the position errors of the injector in three axes. As seen from the results, the largest trajectory error is about 15 $\mu$m after combining errors of three axes. Fig. 6(b) shows the injection force and the force error. The largest force error is about 38. $\mu$N.

Fig. 7 illustrates the experimental results of a cell injection process with the proposed controller without vision-based force feedback. The controller in this case is equivalent to a computed torque control. The control gains are $m = \text{diag}\{0.330,0.165,0.1635\}\ \text{N}/(\mu\text{m}\cdot\text{ms}^{-2})$, $b = \text{diag}\{7.143,4.763,5.191\}\ \text{N}/(\mu\text{m}\cdot\text{ms}^{-1})$, $k = \text{diag}\{9.049, 7.144,10.855\}\ \text{N}/\mu\text{m}$. Fig. 7(a) illustrates the position errors of the injector in three axes, where the largest trajectory error was reduced to about 6 $\mu$m. Fig. 7(b) shows the injection force and the corresponding force error. The maximum force error was reduced to about 18. $\mu$N.

Fig. 8 illustrates the experimental results with the proposed visual-based impedance control. The injection force applied to the cell during the injection process can be regulated with the visual-based force feedback and the desired impedance in the controller. The largest trajectory error was reduced to about 2 $\mu$m, as shown in Fig. 8(a). Fig. 8(b) illustrates the visual force feedback during the piercing phase based on the visual observation, and the maximum force error was reduced to about 14 $\mu$N. In terms of the magnitudes of the maximum position and force errors, the proposed visual based impedance control exhibits the improved motion and force performance compared with the other two control methods.

## V. Conclusion

In this work, a robotic cell injection system with proposed a vision-based force regulation methodology is presented. The injection force is initially calibrated using a planar cell injection task to derive the relationship between the force and the cell deformation, where a cell membrane point-load model is utilized. Further, since the cell deformation is generally difficult to measure directly in an out-of-plane injection task, a relationship between the injection force and the injector visual displacement inside the cell is derived for easy implementation. With the estimated injection force, an impedance control methodology

is developed. An injection motion planning methodology is also proposed in this study. Significantly, experimental results clearly demonstrate the effectiveness of the proposed approach.

## REFERENCES


[1] J. Kuncova and P. Kallio, "Challenges in capillary pressure microinjection," in *Proc. IEEE Int. Conf. EMBS*, 2004, pp. 4998–5001.

[2] Y. Sun and B. J. Nelson, "Biological cell injection using an autonomous microrobotics system," *Int. J. Robot. Res.*, vol. 21, pp. 861–868, 2002.

[3] K. Yanagida, H. Katayose, H. Yazawa, Y. Kimura, K. Konnai, and A. Sato, "The usefulness of a piezo-micromanipulator in intracytoplasmic sperm injection in humans," *Hum. Reprod.*, vol. 14, no. 2, pp. 448–453, 1998.

[4] T. Nakayama, H. Fujiwara, K. Tastumi, K. Fujita, T. Higuchi, and T. Mori, "A new assisted hatching technique using a piezo-micromanipulator," *Fertil. Steril.*, vol. 69, no. 4, pp. 784–788, 1998.

[5] L. Mattos, E. Grant, and R. Thresher, "Semi-automated blastocyst microinjection," in *Proc. IEEE Int. Conf. Robot. Automat.*, 2006, pp. 1780–1785.

[6] K. K. Tan and S. C. Ng, "Computer-controller piezoactuator for cell manipulation," *Proc. Inst. Elect. Eng.*, vol. 150, no. 1, 2003.

[7] D. H. Kim, S. Yun, and B. Kim, "Mechanical force sensor response of single living cells using a microrobotic system," in *Proc. IEEE Int. Conf. Robot. Automat.*, 2004, pp. 5013–5018.

[8] S. Y. Cho and J.-H. Shim, "A new micro biological cell injection system," in *Proc. IEEE Int. Conf. Intell. Robot. Syst.*, 2004, pp. 1642–1647.

[9] K. W. C. Lai, C. C. H. Kwong, and W. J. Li, "KL probes for robotic-based cellular nano surgery," in *Proc. IEEE Conf. Nanotechnol.*, 2003, pp. 152–155.

[10] Y. Sun, K. T. Wan, K. P. Roberts, J. C. Bischof, and B. J. Nelson, "Mechanical property characterization of mouse zona pellucida," *IEEE Trans. Nanobiosci.*, vol. 2, pp. 279–286, 2003.

[11] X. J. Zhang, S. Zappe, R. W. Bernstein, C. C. Chen, O. Sahin, M. Fish, M. P. Scott, and O. Solgaard, "Micromachined silicon force sensor based on diffractive optical encoders for characterization of microinjection," *Sens. Actuators A*, vol. 114/2–3, pp. 197–203, 2004.

[12] F. Beyeler, A. P. Neild, S. Oberti, D. J. Bell, Y. Sun, J. Dual, and B. J. Nelson, "Monolithically fabricated micro-gripper with integrated force sensor for manipulating micro-objects and biological cells aligned in an ultrasonic field," *IEEE/ASME J. Micro. Syst.*, vol. 16, no. 1, pp. 7–15, 2007.

[13] M. A. Greminger and B. J. Nelson, "Vision-based force measurement," *IEEE Trans. Pattern Anal. Machine Intell.*, vol. 26, no. 3, pp. 290–298, 2004.

[14] Y. H. Anis, J. K. Mills, and W. L. Cleghorn, "Visual measurement of MEMS microassembly forces using template matching," in *Proc. IEEE Int. Conf. Robot. Automat.*, 2006, pp. 275–280.

[15] Y. T. Shen, N. Xi, U. C. Wejinya, W. J. Li, and J. Z. Xiao, "Infinite dimension system approach for hybrid force/position control in micromanipulation," in *Proc. IEEE Int. Conf. Robot. Automat.*, 2004, pp. 2912–2917.

[16] B. Nelson, Y. Zhou, and B. Vikramaditya, "Sensor-based micro-assembly of hybrid MEMS devices," *IEEE Contr. Syst. Mag.*, vol. 18, pp. 35–45, 1998.

[17] X. Y. Liu, Y. Sun, W. H. Wang, and B. M. Lansdorp, "Vision-based cellular force measurement using an elastic microfabricated device," *J. Micromech. Microeng.*, vol. 17, pp. 1281–1288, 2007.

[18] H. B. Huang, D. Sun, J. K. Mills, and W. J. Li, "Visual-based impedance force control of three-dimensional cell injections system," in *Proc. IEEE Int. Conf. Robot. Automat.*, 2007, pp. 4196–4201.

[19] H. Huang, D. Sun, J. K. Mills, and S. H. Cheng, "Robotics cell injection system with vision and force control: Towards automatic batch biomanipulation," *IEEE Trans. Robot.*, vol. 25, 2009.

[20] Y. Tan, D. Sun, W. Huang, and S. H. Cheng, "Mechanical modeling of biological cells in microinjection," *IEEE Trans. Nanobiosci.*, vol. 7, pp. 257–266, Dec. 2008.

[21] D. Sun and Y. H. Liu, "Modeling and impedance control of a two-manipulator system handling a flexible beam," *ASME J. Dyn. Syst., Meas., Contr.*, vol. 119, no. 4, pp. 736–742, 1997.

[22] D. H. Kim, Y. Sun, S. Yun, C. N. Hwang, S. Lee, B. Kim, and B. J. Nelson, "Mechanical analysis of chorion softening in prehatching stages of zebrafish embryos," *IEEE Trans. Nanobiosci.*, vol. 5, no. 2, pp. 89–94, 2006.